AlInP-Passivated III-V Solar Cells grown by Dynamic Hydride Vapor Phase Epitaxy

Jacob T. Boyer, Kevin L. Schulte, Matthew R. Young, Aaron J. Ptak, and John Simon

National Renewable Energy Laboratory, Golden, CO, 80401, USA

We report the development of AlInP-passivated solar cells grown by D-HVPE with AM1.5G efficiencies of 26.0% for single junction (1J) GaAs cells, and 28.0% for GaInP/GaAs (2J) tandems. We compare the device performance of solar cells passivated with AlInP vs. control cells passivated with GaInP, which has already enabled near unity carrier collection in GaAs solar cells. 1J devices passivated with either AlInP or GaInP have an identical open circuit voltage (V_{OC}) of 1.06 V and long wavelength current collection near 95%, indicating that both window materials provide a similar degree of passivation. Adding AlInP passivation to each solar cell structure improves the current collection by 1.3 mA/cm^2 and 1 mA/cm^2 for the 1J and 2J, respectively. The AlInP also results in a top cell V_{OC} boost of ~40 mV relative to a tandem device passivated only by a thin, highly-doped GaInP emitter. Secondary ion mass spectrometry measurements indicate that although O and Si both incorporate in the AlInP window, they do not appear in the subsequently grown absorber layers and do not impact its ability to passivate the front surface. We expect these achievements, along with continued optimization, will enable parity of HVPE-grown device efficiencies with state-of-the-art devices grown by other epitaxial methods in the near future.

Keywords: III-V Semiconductors, Tandem Solar Cell, AlInP, Hydride Vapor Phase Epitaxy

1. Introduction

Dynamic hydride vapor phase epitaxy (D-HVPE) is an epitaxial growth method with the potential for high-throughput and low-cost production of III-V photovoltaics and a wide variety of III-V optoelectronic devices [1]. Historically, HVPE growth of Al-containing materials, especially Al(Ga)InP, was deemed impossible due to precursor incompatibilities with reactor hardware and unfavorable growth thermodynamics [2]. However, recent work employing $AlCl_3$, an alternative Al-containing-precursor to AlCl, and uncracked hydrides resulted in the successful growth of AlGaAs and Al(Ga)InP materials in the HVPE environment [3], [4]. In addition, Al-containing materials were successfully integrated in III-V solar cell devices as passivating AlGaAs [5] and AlGaInP [4] [6] window layers. This led to a conversion efficiency as high as 28.3% for a GaInP/GaAs dual junction cell that utilized AlGaInP as both the window and back surface field layers for the GaInP top cell [6]. AlInP, however, has less parasitic optical absorption of short wavelength photons than AlGaInP, and would improve short wavelength current collection beyond the ~550 nm absorption cutoff observed by Shoji, *et al*. [4]. This is due to the large band gap of AlInP (~475 – 500 nm) [7], [8], which is wider than all other III-V alloys at the GaAs lattice constant. Consequently, AlInP is routinely used in the highest efficiency III-V solar cells grown by other methods, such as organometallic vapor phase epitaxy (OMVPE) [9], [10]. However, AlInP is highly susceptible to O contamination [11] and subsequent carrier removal resulting in degraded electronic material quality and passivation ability [12]. One recent study observed high Si and O concentrations in HVPE-grown AlGaInP material and attributed their origins to byproducts from

the reaction of $AlCl_x$ with quartz reactor components and ambient O stemming from the atmospheric pressure HVPE system, respectively [4]. Given this challenge, high-quality passivation by D-HVPE-grown AlInP windows, which has a higher potential for O incorporation [11], has yet to been demonstrated.

Here, we demonstrate AlInP-passivated GaAs single junction (1J) and GaInP/GaAs tandem (2J) solar cells grown by D-HVPE. We characterize the material quality of HVPE-grown AlInP using spectroscopic ellipsometry, atomic force microscopy (AFM), and secondary ion mass spectrometry (SIMS). We then evaluate the performance of AlInP-passivated solar cells relative to control cells passivated with GaInP, which previously demonstrated excellent passivation in 1J devices [13], and show that AlInP enables equal passivation and thus higher current collection in HVPE-grown GaAs cells. Equivalent open circuit voltage (V_{OC}) and fill factor of the 1J devices suggest that both windows provide the same levels of passivation. In the 2J device, adding an AlInP window improves both current collection and top cell voltage compared to our previous use of a thin, highly-doped GaInP emitter as the front-surface passivation. SIMS reveals significant levels of O and Si impurities contained within the AlInP window, although the solar cell results suggest that the observed levels do not impact any aspect of solar cell performance. Thus, we demonstrate that D-HVPE-grown AlInP is indeed of sufficient quality to passivate high-efficiency III-V solar cells.

2. Methods

2.1. Solar cell growth by HVPE

Solar cells were grown using an atmospheric pressure, dual-growth-chamber D-HVPE reactor described previously [13]. GaCl and InCl precursors were generated *in situ* by flowing HCl over elemental Ga and In in the source zones, which were held at 800°C. $AlCl_3$ was generated *ex situ* in a separate quartz ampoule that was redesigned relative to our previously reported Al generator [3] to move the Al source closer to the point of use. The Al ampoule was held at 400°C where generation of $AlCl_3$ is thermodynamically preferential to AlCl [14]. HCl was supplied to the Al source at a partial pressure of ~4×10^{-3} atm to generate $AlCl_3$; InCl was supplied at ~1.4×10^{-4} atm. A total H_2 carrier flow of 2500 sccm was used to quickly transport the $AlCl_3$ through the 800°C source zones in a 4 mm inner diameter quartz tube, similar to a prior report [3]. Group V elements were supplied by AsH_3 and PH_3 gas. AlInP layers were grown in a hydride enhanced regime [15], using a PH_3 carrier flow rate of 2500 sccm to deliver predominantly uncracked PH_3 through another 4 mm inner diameter tube to the growth surface [3]. PH_3 partial pressures of either 2 or 9×10^{-3} atm were used to grow good quality AlInP at growth rates of ~2 µm/min and ~7 µm/min, respectively. The slower rate was used to allow adequate time for changing precursor gases in the other growth chamber for structures containing different layers on either side of the AlInP window. Diethylzinc and H_2Se were used for p- and n-type doping, respectively. Thick layers (e.g. GaInP and GaAs base layers) were grown at 60 µm/h, while the remaining, thinner layers were typically grown at 2 to 7 µm/h.

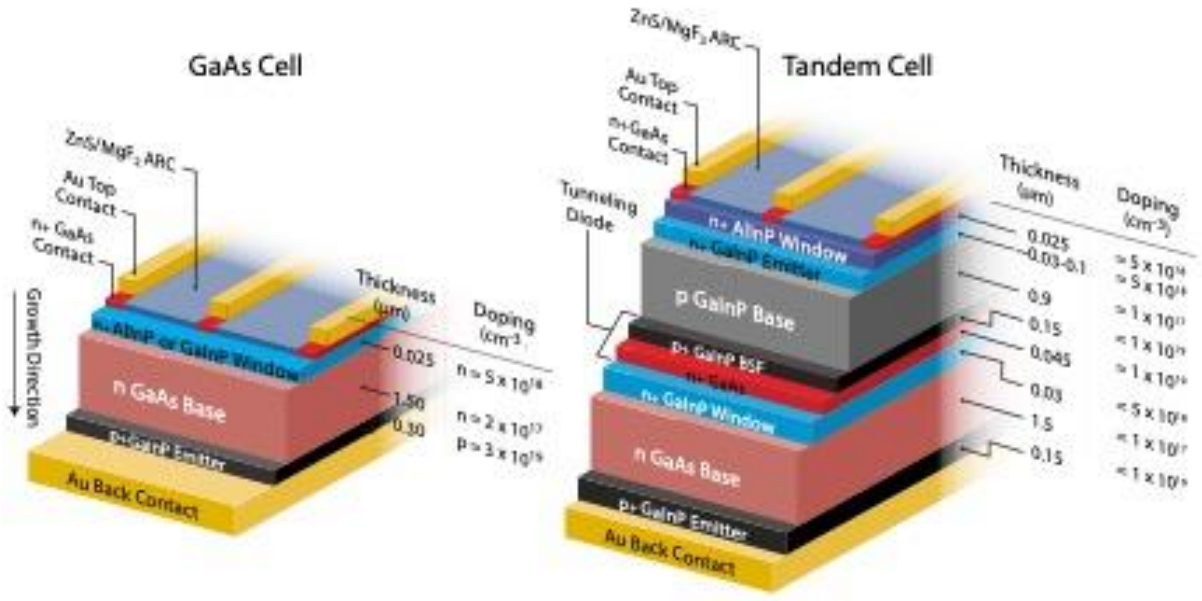

Figure 1: Schematic of the inverted GaAs (1J) and GaInP/GaAs tandem (2J) solar cells, passivated with either GaInP or AlInP, analyzed in this study.

All samples were grown on epi-ready (100)-GaAs wafers with a 6° offcut toward (111)A. The substrate temperature was 650°C during growth. AlInP calibration samples were grown on homoepitaxial GaAs buffers. Active solar cell layers were grown in the inverted sense with structures depicted in Figure 1. The 1J GaAs cell and GaAs bottom subcell of the 2J tandem cell utilized a rear heterojunction structure. The GaInP top subcell of the 2J employed a front homojunction. A homoepitaxial n-GaAs buffer layer followed by a ~200 nm n-GaInP etch stop layer, not shown in these schematics, were grown prior to the active solar cell layers and were removed during device fabrication. Devices employed either AlInP or GaInP windows, grown at 5 μm/h or 2 μm/h, respectively. Both windows were doped n-type to a carrier concentration of ~5×10^{18} cm^{-3}, verified with the electrochemical capacitance-voltage technique, and were grown ~25 nm thick. The GaInP-passivated 2J employed only a thin ~30-nm-thick n-GaInP emitter, which was found to optimize current collection at the expense of increased sheet resistance [16]. The AlInP-passivated 2J employed a thicker ~100 nm emitter to decrease the sheet resistance. A p^+-GaInP layer served as both the back contact and rear emitter in the GaAs cells [9], [17] or the back surface field (BSF) of the GaInP top cell and p-type side of the tunnel junction in the 2J. An Au layer served as both the back contact and rear-reflector to improve collection of photons near the GaAs band edge [17]. It should be noted that the layer doping and thicknesses are nominal targets. The actual values may vary slightly due to dopant diffusion as detailed in a recent report [16].

2.2. Material and device characterization

Differential contrast optical microscopy and AFM were used to characterize the epitaxial film morphology. Growth rates were measured by a combination of contact profilometry, spectroscopic ellipsometry, and/or optical reflectance measurement techniques on calibration samples. Ellipsometry was performed on a J.A. Woollam M-2000DI variable angle spectroscopic

ellipsometer using an angle of incidence ranging from 65° to 80°. SIMS data were taken using a Cameca IMS 7f instrument tuned to minimize background signals while maintaining good detection limits for the elements of interest. SIMS measurements were performed on several calibration and solar cell samples to quantify the dopant and impurity concentrations both within standalone AlInP layers and throughout complete solar cell structures.

Post-growth inversion, substrate removal, and device fabrication were conducted according to methods detailed elsewhere [18], [19]. 0.25 cm^2 devices were defined and fabricated using standard photolithographic techniques. Electroplated Ni/Au and Au were used for the front and back contacts, respectively, with nominally identical thicknesses to cells demonstrated in [13], [16], and [18]. A ZnS/MgF_2 bi-layer antireflective coating (ARC), with layer thicknesses of ~50 nm and ~100 nm, respectively, targeting the optimal current collection of each cell with a 1D transfer matrix method model [20], was evaporated on the cells after device processing.

Solar cell external quantum efficiency (EQE) and reflectance were measured using a custom QE system with lock-in amplification and a monochromated beam that is split between a calibrated reference photodetector and the device under test. Current density-voltage (*J-V*) characteristics were certified by the National Renewable Energy Laboratory Photovoltaic Device Performance Group. All EQE spectra were scaled to yield the same AM1.5G-integrated J_{SC} as that obtained from the certified illuminated *J-V* results. Electroluminescence (EL) analysis after Geisz, *et al.* [15] was conducted in conjunction with standard dark *J-V* measurements to calculate *J-V* curves for the individual subcells in the 2J devices, and to extract implied V_{OC} and dark current contributions for each subcell, as exampled in Schulte, *et al.* [18].

3. Results and Discussion

3.1. AlInP material characterization

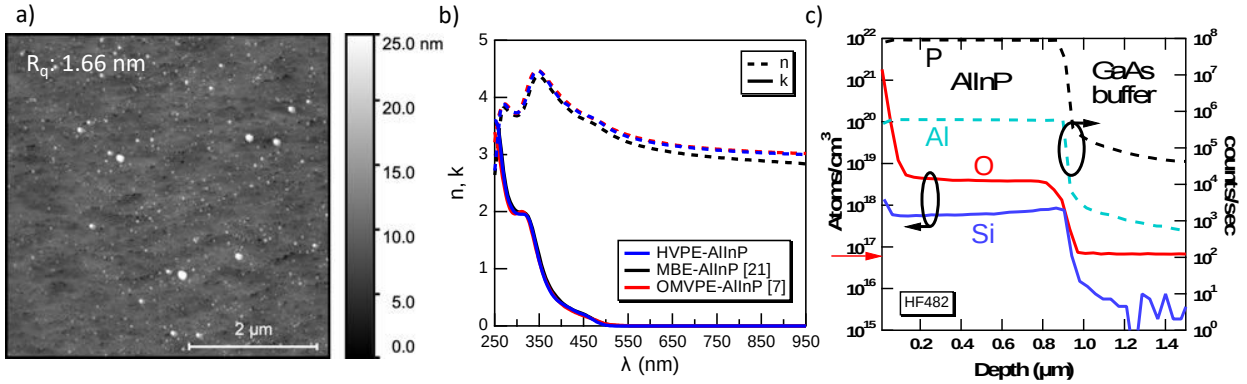

Figure 2: a) atomic force micrograph and b) optical n and k spectra obtained from spectroscopic ellipsometry of a typical ~300-nm-thick HVPE-grown AlInP standalone film. The optical spectra of MBE-grown [21] and OMVPE-grown [7] AlInP are presented for reference. c) SIMS depth profiles obtained on a 1 µm-thick HVPE-grown AlInP film. The red arrow indicates the O background level in the SIMS instrument.

First, we demonstrate the material quality of our HVPE-grown AlInP. Figure 2a shows an atomic force micrograph of a ~300-nm-thick AlInP film lattice-matched to GaAs with an R_q value of 1.66 nm obtained on a 5 µm × 5 µm area. We note that the presence of non-growth-related surface contamination (white spots) contributes to much of the 1.66 nm R_q and that this

represents an upper limit of roughness. Nevertheless, this surface is sufficiently smooth and does not affect the morphology of photovoltaic device layers grown on AlInP windows. Figure 2b shows optical dispersions obtained from spectroscopic ellipsometry on our HVPE-grown films and literature data for AlInP grown by molecular beam epitaxy (MBE) [21] and OMVPE [7]. The optical dispersions closely match and indicate a direct band gap of ~500 nm, suggesting that our D-HVPE-grown AlInP has nominally identical optical properties to AlInP grown by other well-established III-V deposition techniques. Figure 2c shows O and Si concentration depth profiles and secondary-ion signals of Al and P obtained from SIMS analysis of a ~1 µm thick AlInP sample. The depth profiles of Al and P exhibit tails into the GaAs buffer layer due to broadening of the SIMS signal and roughening of the crater during depth profiling. Surface effects account for the high O signal in the first ~100 nm. We observe an average O concentration of 4×10^{18} cm^{-3}, which is slightly higher than the ~2×10^{18} cm^{-3} O level measured in AlGaInP by Shoji, *et al*. [4]. This difference may be caused by the increased potential for O incorporation with the higher Al content in AlInP [11], although differences in growth conditions could also explain this finding. Similar to Shoji, *et al.* [4], we observe a delay in O incorporation at the start of the AlInP growth relative to Si, suggesting that O incorporation is controlled by a surface segregation mechanism as suggested previously [4] [22], whereby O segregation flux opposes O incorporation flux until the O concentration at the surface becomes saturated. Si impurities likely stem from a non-negligible concentration of AlCl reacting with reactor quartz. Generation of trace amounts of AlCl is expected in the Al source at 400°C from thermodynamic calculations, and the decomposition of $AlCl_3$ to AlCl and HCl is possible as the $AlCl_3$ molecule passes through the 800°C source zone or when the $AlCl_3$ interacts with the substrate surface. We cannot discern between AlCl generated in the source or AlCl generated from $AlCl_3$ decomposition with the present data. The Si in our case decays slightly into the AlInP layer to an average concentration of ~6×10^{17} cm^{-3}, which could suggest a higher concentration of Si occurs at the start of the AlInP growth. This average concentration is lower than the ~5×10^{18} cm^{-3} that was reported in AlGaInP, which could indicate less $AlCl_x$ etching of the reactor quartz, although differences in reactor design and growth conditions, especially Al source temperature, could also explain this finding.

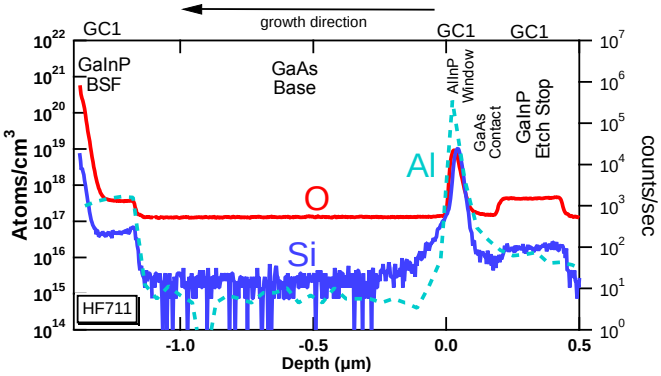

Figure 3: SIMS depth profiles of O and Si measured in a GaAs (1J) solar cell structure near the window to absorber interface. O is at or below background levels in all layers except the AlInP window.

We used similar growth conditions as the AlInP shown in Figure 2 in the inverted rear heterojunction 1J GaAs device structures described above. Figure 3 shows SIMS spectra that highlight the AlInP window and GaAs base region of a typical solar cell stack. The Al depth profile indicates the position of the AlInP/GaAs interface. Here, the Al tail into the GaAs base is near the

detection limit. The AlInP window contains O and Si impurities at lower and higher levels, respectively, to those in the standalone AlInP shown in Figure 2c. The Si depth profile peaks at ~1×10^{19} cm^{-3} and tails somewhat into the n-GaAs absorber. Here, the Si concentration is higher than that in the thick epilayer presented in Figure 2c, which is possibly due to slight differences in growth conditions, such as V/III ratio. We observe slight Si incorporation into the GaAs base, although we cannot distinguish between the possible mechanisms of Si diffusion, crosstalk of gas streams between chambers, or Si atoms acting as a surfactant given the present data. We observe some Al in the GaInP emitter, which was grown in the same chamber (GC1) as the AlInP. These levels were too small to quantify by other techniques. The overall Si concentration in the etch stop layers is at the typical background level of ~3×10^{16} cm^{-3}. The GaInP emitter appears to have more Si than this background level. This may indicate that the AlInP window grown prior causes Al and Si contamination, albeit to a lesser degree than that observed by Shoji, *et al.* [6]. The O concentration peaks at ~2×10^{18} cm^{-3} and then decays rapidly to the instrument background in the subsequently grown GaAs absorber. This result is consistent with those of a prior study that observed low O incorporation within epitaxial GaAs in the presence of surface segregated O and ambient O [22]. O remains below the detection limits in the other layers, including the GaInP emitter. Note that the relative sensitivity factor of O in GaAs is different from O in GaInP, thus the detection limit is higher in GaInP. Surface segregation may also account for the lower O concentration in the AlInP because this thin layer is grown before the O concentration has saturated to the level that we observed in the much thicker AlInP shown in Figure 2c.

3.2. 1J device characterization

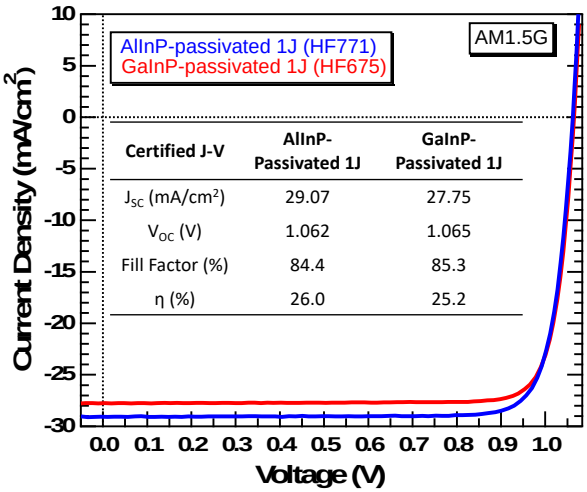

Figure 4: Certified illuminated *J-V* characteristic and extracted metrics of AlInP- and GaInP-passivated GaAs (1J) solar cells under a simulated AM1.5G spectrum.

Next, we compared the photovoltaic performance of 1J devices passivated by AlInP with control devices passivated by GaInP, which were previously demonstrated to enable near unity carrier collection in 1J devices [13]. We applied AlInP to inverted rear-junction solar cells because this structure is generally more sensitive to the quality of surface passivation [23] than front-junction solar cells [24], and the sensitive, active layers are grown after the AlInP. Figure 4 shows the certified AM1.5G illuminated *J-V* characteristic and extracted solar cell metrics of both devices. The certified efficiency of the AlInP-passivated device was (26.03 ± 0.19)%, which is the highest

reported efficiency reached by any single junction HVPE-grown solar cell. Both devices yield V_{OC} of ~1.06 V and ~84-85% fill factors indicating similar material quality. The AlInP-passivated solar cell exhibits a 1.3 mA/cm^2 increase in certified J_{SC} over the GaInP-passivated cell. We then evaluated the quantum efficiency of these solar cells to better understand where the improvement in current density originates. Figure 5 compares the EQE of both devices. The AlInP-passivated device exhibits an increase in short wavelength (< 650 nm) current collection relative to the GaInP-passivated control. The increased short wavelength optical transparency of the AlInP window accounts for effectively all of the 1.3 mA/cm^2 improvement in J_{SC} as determined by integration of the EQEs with the AM1.5G spectrum. In the long wavelength region, the EQE is >95%, indicating nearly perfect collection of absorbed photons below the absorption edge of either window. This high degree of collection cannot be obtained if the window/base interface recombination velocity (IRV) is large because these are rear junction cells [25]. The roughly 4% of EQE loss could be attributed to non-zero IRV and/or limited minority carrier diffusion length in the GaAs base. Separating these factors will require deeper study, but we note that the equal long-wavelength current collection and invariant V_{OC} suggest excellent passivation and very similar IRV values for the two different window layers used in these devices. Thus, we find that both windows sufficiently passivate these rear-junction GaAs solar cells, despite the high levels of O and Si observed in the SIMS measurements of the AlInP window. The parity V_{OC} and fill factor values observed between the devices also suggest that the AlInP window does not alter either bulk recombination in the GaAs absorber or recombination at the heterojunction. Therefore, we conclude that the presence of AlInP has no impact on the electrical performance of subsequently grown layers.

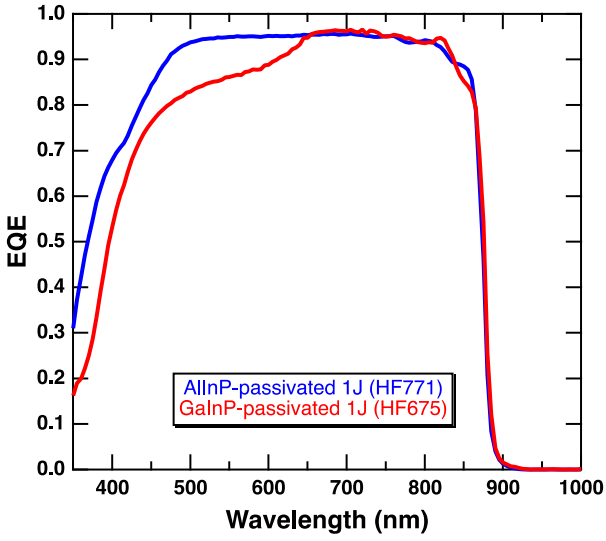

Figure 5: EQE measurements of D-HVPE-grown rear heterojunction GaAs (1J) solar cells passivated with either AlInP or GaInP window layers.

3.3. 2J device characterization

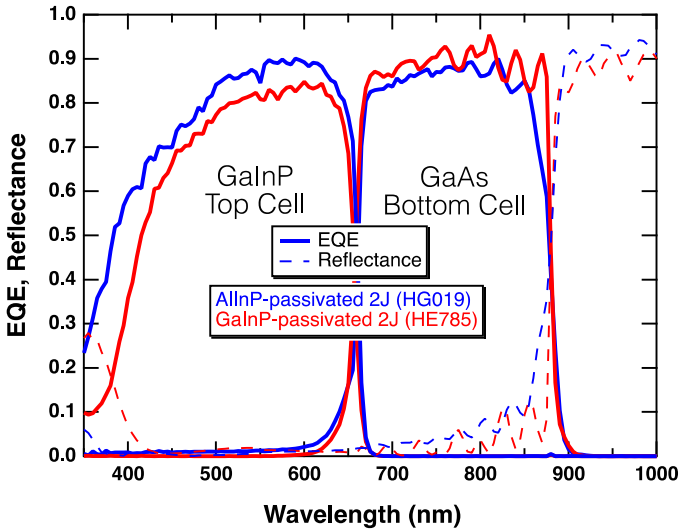

Figure 6: EQE and reflectance of GaInP/GaAs (2J) solar cells grown by D-HVPE.

Next, we evaluated the performance of 2J solar cells with and without AlInP passivation of the GaInP top cell. Figure 6 shows the EQE of the 2J solar cells. The AlInP window increases short wavelength current collection (< 650 nm) by reducing the parasitic absorption that occurs when employing the n-GaInP emitter as the passivating layer for the p-GaInP base. Here, we use the nomenclature 'GaInP-passivated' for simplicity, although in this case the emitter is effectively unpassivated because it lacks a minority carrier barrier to reflect carriers away from the front surface. Therefore, adding a discrete AlInP window both improves passivation and enables collection of photons in the emitter that would otherwise be uncollected [18]. Both of these factors result in an improvement in current collection, which spans the whole wavelength range of the top cell because previously uncollected photons in the unpassivated emitter are now collected. Both bottom cells show similar EQE response, although differences in the reflectance cause a slight reduction for the AlInP-passivated case. We find both cells are close to current matched, given that the difference in current collection between each subcell, obtained by integrating the EQE with the AM1.5G spectrum, is within the roughly ±0.3 mA measurement error of the EQE.

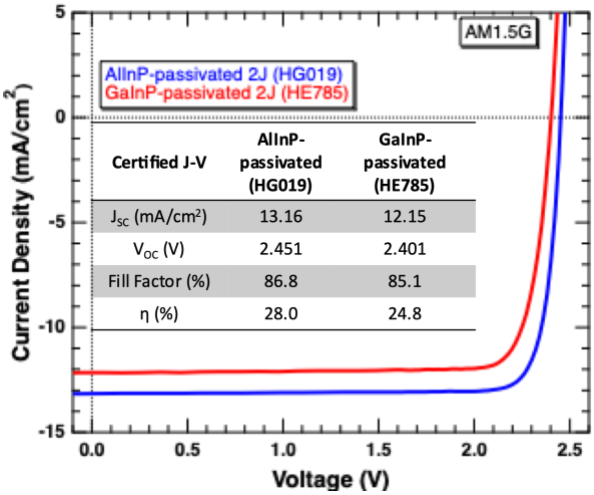

Certified J-V	AlInP-passivated (HG019)	GaInP-passivated (HE785)
J_{SC} (mA/cm²)	13.16	12.15
V_{OC} (V)	2.451	2.401
Fill Factor (%)	86.8	85.1
η (%)	28.0	24.8

Figure 7: Illuminated *J-V* characteristics of GaInP/GaAs (2J) solar cells. Figures of merit are given in the inset table.

Figure 7 shows the illuminated *J-V* characteristic and extracted solar cell metrics of the 2J solar cells. Here, the AlInP-passivated 2J reaches a certified efficiency of 28.0%, which is a >3% absolute increase relative to the GaInP-passivated case. The J_{SC} improves by 1.0 mA/cm^2 due to the improvement in the top cell passivation and the fill factor increases by almost 2% relative to the control despite improved current matching relative to the GaInP-passivated device. This improvement is explained by reduced series resistance in the AlInP-passivated device, as indicated by a change in slope of the *J-V* near V_{OC}. The AlInP passivation enabled the use of a thicker emitter, ~3× thicker in this case, which led to a ~3× lower sheet resistance, lower series resistance, and improved fill factor. Furthermore, the V_{OC} of the AlInP-passivated device improves by 50 mV relative to the control.

Subcell:	GaAs Bottom Cell		GaInP Top Cell	
Device:	GaInP-passivated 2J	AlInP-passivated 2J	GaInP-passivated 2J	AlInP-passivated 2J
V_{OC} (V)	1.027	1.037	1.376	1.416

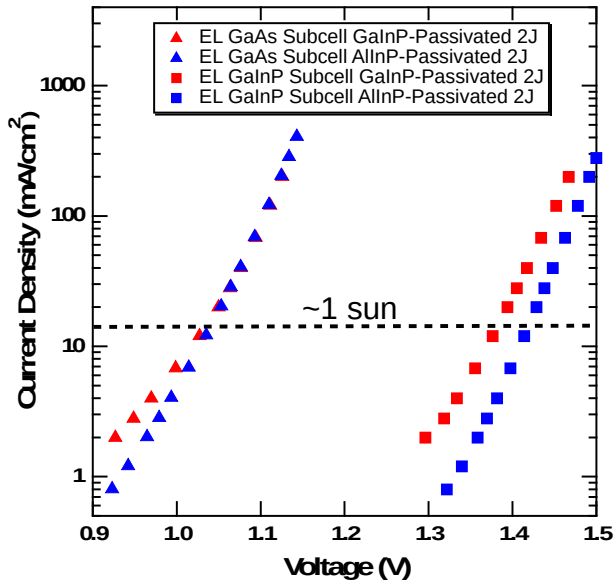

Figure 8: EL-derived *J-V* characteristic of GaInP/GaAs (2J) solar cells. V_{OC} at 1 sun are given in the table.

Finally, we analyzed EL-derived *J-V* data to understand the origin of this observed V_{OC} boost. Figure 8 shows dark *J-V* curves, calculated from the EL of each subcell measured over a range of injected current densities. We extracted the implied V_{OC} of each subcell at the J_{SC} of the corresponding tandem device. The AlInP passivation improves the top cell V_{OC} from 1.376 V to 1.416 V, which accounts for most of the V_{OC} difference in the 2J light *J-V* curves. We attribute this 40 mV increase to the suppression of surface recombination currents when adding an AlInP window. The bottom cells each show V_{OC} ~1.03 V.

At 28.0% conversion efficiency this AlInP-passivated 2J surpasses the 26.9% efficient AlGaInP-passivated 2J demonstrated by Shoji et al. [4]. The AlInP-passivated 2J is near to the 28.3% efficient AlGaInP-passivated 2J that Shoji et al. demonstrated after adding an AlGaInP BSF,

which yielded an additional improvement in V_{OC} [6]. We expect to observe a similar boost in V_{OC} by integrating an AlGaInP BSF into our current structure. Our AlInP-passivated 2J serves as an initial demonstration upon which the addition of wider bandgap BSF and tunnel junction layers will improve photoconversion efficiencies toward state-of-the-art.

4. Conclusion

We demonstrated that the inclusion of AlInP windows in both GaAs (1J) and GaInP/GaAs (2J) III-V solar cells grown by D-HVPE leads to improved photoconversion efficiencies without degrading any of the individual cell metrics. These cells reach 26.0% and 28.0% certified AM1.5G efficiencies for AlInP-passivated 1J and 2J devices, respectively. In the 1J cells, the invariant long wavelength EQE, FF, and V_{OC} suggest that the passivation performance of D-HVPE-grown AlInP is equivalent to GaInP, and that the AlInP does not degrade subsequently grown layers in any way. We show that while AlInP does incorporate O and Si impurities, the levels of these impurities do not prevent the attainment of passivation nor hinder any other aspect of solar cell performance. Thus, we conclude that the material quality of D-HVPE-grown AlInP is indeed sufficient for integration in high-efficiency photovoltaics and that attaining state-of-the-art efficiencies is not limited by fundamental materials growth challenges.

Acknowledgements

The authors would like to acknowledge David Guiling for materials growth and Evan Wong for cell processing. This work was authored in part by the National Renewable Energy Laboratory, operated by Alliance for Sustainable Energy, LLC, for the U.S. Department of Energy (DOE) under Contract No. DE-AC36-08GO28308. The information, data, or work presented herein was funded by the DOE's Office of Energy Efficiency and Renewable Energy (EERE) under Solar Energy Technologies Office (SETO) Agreement Number 34358. NREL acknowledges support from the Operational Energy Capability Improvement Fund (OECIF) of the U.S. Department of Defense (DOD). The authors wish to thank R. Darling of the Office of the Undersecretary of Defense for Acquisition and Sustainment, Arlington, VA, USA for guidance and support. The views expressed in the article do not necessarily represent the views of the DOE or the U.S. Government.

References

[1] J. Simon, K. Schulte, K. Horowitz, T. Remo, D. Young, and A. Ptak, "III-V-Based Optoelectronics with Low-Cost Dynamic Hydride Vapor Phase Epitaxy," *Crystals*, vol. 9, no. 1, p. 3, Dec. 2018, doi: 10.3390/cryst9010003.

[2] G. B. Stringfellow, "VPE Growth of III/V Semiconductors," *Annu. Rev. Mater. Sci.*, vol. 8, no. 1, pp. 73–98, Aug. 1978, doi: 10.1146/annurev.ms.08.080178.000445.

[3] K. L. Schulte *et al.*, "Growth of AlGaAs, AlInP, and AlGaInP by Hydride Vapor Phase Epitaxy," *ACS Appl. Energy Mater.*, vol. 2, no. 12, pp. 8405–8410, Dec. 2019, doi: 10.1021/acsaem.9b02080.

[4] Y. Shoji, R. Oshima, K. Makita, A. Ubukata, and T. Sugaya, "InGaP/GaAs dual-junction solar cells with AlInGaP passivation layer grown by hydride vapor phase epitaxy," *Prog Photovolt Res Appl*, p. pip.3454, Jul. 2021, doi: 10.1002/pip.3454.

[5] W. Metaferia, K. L. Schulte, J. Simon, D. Guiling, and A. J. Ptak, "Demonstration of passivation using a low-temperature-grown, Al-containing window layer by HVPE," in *2020 47th IEEE Photovoltaic Specialists Conference (PVSC)*, Calgary, AB, Canada, Jun. 2020, pp. 0672–0674. doi: 10.1109/PVSC45281.2020.9300791.

[6] Y. Shoji, R. Oshima, K. Makita, A. Ubukata, and T. Sugaya, “28.3% Efficient III–V Tandem Solar Cells Fabricated Using a Triple-Chamber Hydride Vapor Phase Epitaxy System,” *Solar RRL*, p. 2100948, Dec. 2021, doi: 10.1002/solr.202100948.
[7] E. Ochoa-Martínez *et al.*, “Refractive indexes and extinction coefficients of n- and p-type doped GaInP, AlInP and AlGaInP for multijunction solar cells,” *Solar Energy Materials and Solar Cells*, vol. 174, pp. 388–396, Jan. 2018, doi: 10.1016/j.solmat.2017.09.028.
[8] J. S. Cheong, J. S. Ng, A. B. Krysa, J. S. L. Ong, and J. P. R. David, “Determination of absorption coefficients in AlInP lattice matched to GaAs,” *J. Phys. D: Appl. Phys.*, vol. 48, no. 40, p. 405101, Oct. 2015, doi: 10.1088/0022-3727/48/40/405101.
[9] S.-T. Hwang *et al.*, “Bandgap grading and Al0.3Ga0.7As heterojunction emitter for highly efficient GaAs-based solar cells,” *Solar Energy Materials and Solar Cells*, vol. 155, pp. 264–272, Oct. 2016, doi: 10.1016/j.solmat.2016.06.009.
[10] M. A. Steiner *et al.*, “High Efficiency Inverted GaAs and GaInP/GaAs Solar Cells With Strain-Balanced GaInAs/GaAsP Quantum Wells,” *Adv. Energy Mater.*, vol. 11, no. 4, p. 2002874, Jan. 2021, doi: 10.1002/aenm.202002874.
[11] S. A. Stockman *et al.*, “Oxygen incorporation in AlInP, and its effect on P-type doping with magnesium,” *Journal of Elec Materi*, vol. 28, no. 7, pp. 916–925, Jul. 1999, doi: 10.1007/s11664-999-0220-x.
[12] K. A. Bertness, S. R. Kurtz, S. E. Asher, and R. C. Reedy, “AlInP benchmarks for growth of AlGaInP compounds by organometallic vapor-phase epitaxy,” *Journal of Crystal Growth*, vol. 196, no. 1, pp. 13–22, Jan. 1999, doi: 10.1016/S0022-0248(98)00751-9.
[13] J. Simon, K. L. Schulte, D. L. Young, N. M. Haegel, and A. J. Ptak, “GaAs Solar Cells Grown by Hydride Vapor-Phase Epitaxy and the Development of GaInP Cladding Layers,” *IEEE J. Photovoltaics*, vol. 6, no. 1, pp. 191–195, Jan. 2016, doi: 10.1109/JPHOTOV.2015.2501723.
[14] Y. Kumagai, T. Yamane, T. Miyaji, H. Murakami, Y. Kangawa, and A. Koukitu, “Hydride vapor phase epitaxy of AlN: thermodynamic analysis of aluminum source and its application to growth,” *phys. stat. sol. (c)*, no. 7, pp. 2498–2501, Dec. 2003, doi: 10.1002/pssc.200303360.
[15] K. L. Schulte, A. Braun, J. Simon, and A. J. Ptak, “High growth rate hydride vapor phase epitaxy at low temperature through use of uncracked hydrides,” Appl. Phys. Lett., vol. 112, no. 4, p. 042101, Jan. 2018, doi: 10.1063/1.5013136.
[16] D. Roberts, J. Simon, K. Schulte, M. R. Young, and A. Ptak, “Dopant Diffusion Control for Improved Tandem Cells Grown by D-HVPE,” *IEEE J. Photovoltaics*, vol. 11, no. 5, pp. 1251–1255, Sep. 2021, doi: 10.1109/JPHOTOV.2021.3095756.
[17] J. F. Geisz, M. A. Steiner, I. García, S. R. Kurtz, and D. J. Friedman, “Enhanced external radiative efficiency for 20.8% efficient single-junction GaInP solar cells,” *Appl. Phys. Lett.*, vol. 103, no. 4, p. 041118, Jul. 2013, doi: 10.1063/1.4816837.
[18] K. L. Schulte, J. Simon, and A. J. Ptak, “Multijunction $Ga_{0.5}In_{0.5}P$/GaAs solar cells grown by dynamic hydride vapor phase epitaxy,” *Prog Photovolt Res Appl*, vol. 26, no. 11, pp. 887–893, Nov. 2018, doi: 10.1002/pip.3027.
[19] A. Duda, S. Ward, and M. Young, “Inverted Metamorphic Multijunction (IMM) Cell Processing Instructions,” NREL/TP-5200-54049, 1036035, Feb. 2012. doi: 10.2172/1036035.
[20] E. Centurioni, “Generalized matrix method for calculation of internal light energy flux in mixed coherent and incoherent multilayers,” *Appl. Opt.*, vol. 44, no. 35, p. 7532, Dec. 2005, doi: 10.1364/AO.44.007532.
[21] W. Yuan and D. C. Hall, “Variable-angle spectroscopic ellipsometry of InAlP native oxide dielectric layers for GaAs metal–oxide–semiconductor field effect transistor applications,” *Journal of Applied Physics*, vol. 113, no. 10, p. 103515, Mar. 2013, doi: 10.1063/1.4794817.
[22] S. Naritsuka, O. Kobayashi, K. Mitsuda, and T. Nishinaga, “Oxygen incorporation mechanism in AlGaAs layers grown by molecular beam epitaxy,” *Journal of Crystal Growth*, vol. 254, no. 3–4, pp. 310–315, Jul. 2003, doi: 10.1016/S0022-0248(03)01181-3.
[23] D. L. Lepkowski, J. T. Boyer, D. J. Chmielewski, A. C. Silvaggio, S. A. Ringel, and T. J. Grassman, “Investigation of Rear-Emitter $GaAs_{0.75}P_{0.25}$ Top Cells for Application to III–V/Si Tandem Photovoltaics,” *IEEE J. Photovoltaics*, vol. 9, no. 6, pp. 1644–1651, Nov. 2019, doi: 10.1109/JPHOTOV.2019.2939069.
[24] S. R. Kurtz, J. M. Olson, D. J. Friedman, J. F. Geisz, K. A. Bertness, and A. E. Kibbler, “Passivation of Interfaces in High-Efficiency Photovoltaic Devices,” *MRS Proc.*, vol. 573, p. 95, 1999, doi: 10.1557/PROC-573-95.

[25] D. L. Lepkowski, T. Kasher, J. T. Boyer, D. J. Chmielewski, T. J. Grassman, and S. A. Ringel, “The Critical Role of AlInP Window Design in III–V Rear-Emitter Solar Cells,” *IEEE J. Photovoltaics*, vol. 10, no. 3, pp. 758–764, May 2020, doi: 10.1109/JPHOTOV.2020.2978863.